Environmental Science & Technology

pubs.acs.org/est

Article

Deposition Patterns of Carbon Black Nanoparticles in Pulmonary Lobes and Airway Generations: Implications for Lung Remodeling

Wenting Cheng,[⊥] Zijian Ma,[⊥] Xinyi Zhang, Yuxin Zheng, Wei Han,* Yingxin Yu,* and Jinglong Tang*

Cite This: https://doi.org/10.1021/acs.est.5c14667

Read Online

ACCESS | Metrics & More | Article Recommendations | Supporting Information

ABSTRACT: Carbon black nanoparticles (CBNPs) pose respiratory risks due to occupational and environmental exposure, yet their spatially heterogeneous effects on lung remodeling remain unclear. We quantified remodeling patterns using high-resolution computerized tomography (HRCT) in 69 carbon black packers and 107 controls, with carbon content in airway macrophages (CCAM) serving as a bioeffective dosimeter. CBNP-exposed workers exhibited elevated mean lung density in the left (β = 7.75 HU) and right upper lobe (β = 6.22 HU, all p values $\leq$ 0.047), showing clear dose-dependent trends with CBNP internal dose. Thickened airway wall area percentage (WA%) was observed in the sixth- and ninth-generation bronchi of the upper lobes, including the sixth-generation left B1 + 2 bronchus (β = 3.76%) and the right B1 bronchus to the carina (β = 4.43%; all p values $\leq$ 0.006). Dose−response trends linked CCAM with WA% thickening in larger sixth-generation bronchi of bilateral upper lobes (all p_{trend} values $\leq$ 0.008), absent in ninth-generation airways. Computational modeling revealed 45.2% higher particle deposition in bilateral upper lobes and 3-fold greater deposition in sixth-generation airways, governed by inertial impaction, which dominates in proximal small airways. This study visualizes region-specific pulmonary remodeling associated with CBNP exposure in humans, identifying the bilateral upper lobes and proximal small airways as key vulnerability hotspots. By linking deposition physics—dominated by inertial impaction—to selective regional targeting, these findings provide mechanistic insight into how nanoparticle deposition patterns translate into heterogeneous lung remodeling. The combined use of quantitative HRCT biomarkers and respiratory tract deposition modeling offers a framework for early surveillance and risk assessment of nanomaterial-induced lung injury.

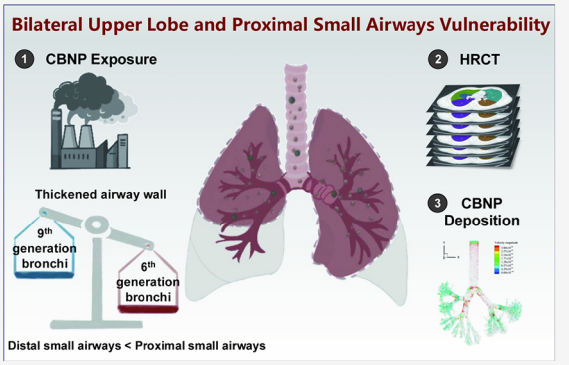

KEYWORDS: *carbon black nanoparticle, lung density, small airway, vulnerability analysis, respiratory tract model, particle deposition*

1. INTRODUCTION

Environmental nanoparticles are increasingly recognized for their respiratory health impacts. Carbon black nanoparticles (CBNPs) are largest production engineered nanoparticles widely used in rubbers, inks, and paints.[1−3] Their production continues to grow, partly driven by the lithium battery industry, where acetylene black serves as a conductive additive.[4,5] Chronic exposure to CBNPs has been associated with increased respiratory symptoms, small opacities on chest radiographs, reduced pulmonary function, and decreased Clara cell secretory protein (CC16).[6−8] These findings suggest structural lung alterations. CBNPs possess small particle size and large surface area,[9] which enhance their reactivity in the respiratory tract. They impair macrophage phagocytic capacity,[10] resist clearance, and induce persistent inflammatory.[6] However, lung function tests lack sensitivity for early structural remodeling at the individual level, and histopathology is rarely feasible in population studies. Thus, the region-specific patterns and dose−response features of long-term CBNP-induced lung remodeling remain unclear.

High-resolution computerized tomography (HRCT) provides a noninvasive, quantitative, and spatially localized technique for visualizing lung structural changes *in vivo*,[11,12] with imaging findings shown to correlate well with histopathological changes in biopsy-based studies.[13−15] Structural indices derived from HRCT, including mean lung density (MLD), low attenuation areas volume percentage (LAA%), and airway wall area percentage (WA%), sensitively capture remodeling of both lung parenchyma and airways.[16,17] Increases in MLD accompanied by reductions in LAA% reflect elevated tissue attenuation, as observed in pathological conditions such as pulmonary edema, fibrosis, and heightened inflammation.[18,19] Airway structure can be further assessed using WA%, defined as the proportion of airway wall area relative to the total airway

Received: October 16, 2025
Revised: April 2, 2026
Accepted: April 2, 2026

area, which reflects relative airway wall thickening and airway remodeling. In our HRCT-based model,[8,20] sixth generation bronchi approximated the ~ 2 mm diameter threshold commonly used to define proximal small airways,[21] whereas ninth generation bronchi represent more distal small airways. Small airways are characterized by narrow lumens, absence of cartilaginous support, and limited clearance capacity, rendering them particularly susceptible to particle deposition and injury. Structural alterations in these airways are increasingly recognized as early and functionally relevant changes that contribute disproportionately to airflow limitation in environmentally and occupationally exposed populations.[14,22]

In this study, we integrated HRCT with multigeneration airway models to characterize the spatially heterogeneous patterns of lung remodeling in workers with long-term CBNP exposure. We identified dose−dependent increases in lung density and airway wall thickening, with selective vulnerability of the bilateral upper lobes and proximal small airways. Deposition simulations further revealed preferential particle retention in these regions, governed by inertial impaction. Together, these findings establish an exposure−deposition−remodeling framework that strengthens mechanistic understanding and supports early surveillance of nanomaterial-induced lung injury.

2. MATERIALS AND METHODS

2.1. Study Subjects

A total of 69 carbon black packers (CBPs) that had bagged newly manufactured CBNPs for more than six months in the acetylene CBNP industry were recruited as the exposed group, whereas 107 workers from local waterworks were recruited as the control group (non-CBPs), establishing the CBP cohort. This study employed a cross-sectional design. The design details, including the inclusion and exclusion criteria, were based on previous reports.[23,24] During the onsite investigation, we specifically chose to conduct a detailed questionnaire survey and comprehensive health examination immediately after the subjects completed their night shift. Biological samples such as sputum were also collected at this time. Additionally, 14 CBPs and 29 non-CBPs did not receive end-inhalation lung CT scanning or incomplete acquisition of lung structural parameters, and 5 non-CBPs did not have a smoking history, which led to a final sample size of 55 CBPs and 73 non-CBPs. All participants voluntarily signed informed consent before the interview and any procedures. The protocol was approved by the Medical Ethical Review Committee of the National Institute for Occupational Health and Poison Control, Chinese Center for Disease Control and Prevention (protocol number: NIOHP201604).

2.2. Characterization of CBNPs and Exposure Assessment

The physicochemical characteristics of CBNPs in this occupational setting have been described previously.[24,25] Environmental exposure assessment was performed using established methods.[6,25] The CCAM assay was quantified according to our previous protocols.[24,26] The percentage of carbon particles to the cytoplasmic area (PCOC) in 50 macrophages per subject was calculated (Figure S1), with upper quartile (Q3) of the PCOC selected as the CCAM index. The CCAM reflects cumulative internal lung dose of inhaled CBNP. Detailed methods are provided in the Supporting Information.

2.3. Quantitative HRCT Assessment of Lung Density and Airway Dimensional Parameters

After rigorous inspiratory breath-hold training by a professional radiologist, each subject was scanned at full inspiration by a 64-slice CT scanner (LightSpeed VCT XT or OPTIMA CT660, GE Healthcare, USA) from the lung apex to the base. CT images were analyzed via the ISP9.0 software package (Philips Diagnostics, Netherlands). Whole lung and bronchial tree images were reconstructed with a high spatial resolution algorithm. The ISP9.0 software automatically segmented the lung lobes and measured the MLD, lung volume and LAA% for both lung, right lung, left lung, and each lobe, including the right upper lobe, right middle lobe, right lower lobe, left upper lobe, and left lower lobe. Airway wall area percentage (WA%) was assessed at the sixth- and ninth-generation bronchi, representing proximal and distal small airways, respectively, which are recognized as key sites of early airway remodeling.[27,28] Measurements were performed along four predefined bronchopulmonary segmental airways: right B1 to carina, right B9 to carina, left B1 + 2 to carina, and left B9 to carina. For each bronchial generation, the average WA% was calculated across the four lung segments (Figure 1). This

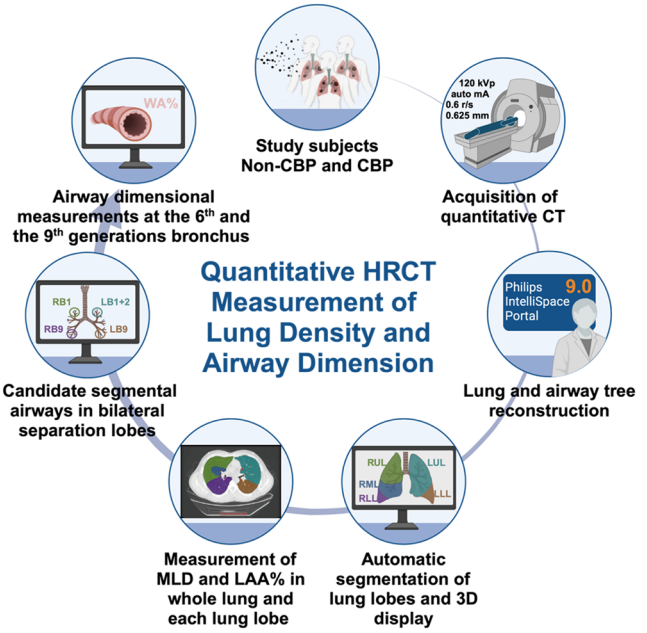

Figure 1. Flowchart of quantitative HRCT determination of lung density and airway dimension.

quantitative HRCT protocol for small airway assessment has been validated in our previous studies, showing high reproducibility and accuracy for measuring sixth- to ninth-generation airway parameters.[8,20] Detailed procedures are provided in the Supporting Information.

2.4. Mathematical Model and Methodology

This study employs a laminar flow model to simulate airflow and CBNP deposition in the lower respiratory tract,[29−32] encompassing ten bronchial generations from the first generation to the tenth generation and five lung lobes, namely, the right upper lobe, right middle lobe, right lower lobe, left upper lobe, and left lower lobe (Figure S2). We adopted laminar flow because our focus is on sixth- and ninth-generation small airways, where airflow is inherently laminar.[30,31] Considering our previous model,[33−35] airflow was treated as transient and incompressible, with the fluid phase governed by the continuity, momentum, and energy equations, as well as the discrete phase governed by Brownian motion, the Stokes−Cunningham drag law, and gravitational forces, which is generalizable to other nanomaterials, as it relies on universal deposition mechanisms and standard airway anatomy. The reliability of the model results has been discussed in our previous research.[34] CBNP properties were defined on the basis of our previous experimental data and workplace characterization: the particle diameter ranged from 200 to 400 nm (Table S1), with field measurements revealing about 96.67% CBNPs were <1 μm and >50% particles were <0.523 μm; the particle density was set at 2.0 g/mL per breath.[6,24] This 200−400 nm size range represents the dominant respirable CBNP fraction that preferentially deposits in the sixth- and ninth-generation small airways, the key anatomical focus of our HRCT imaging analysis, thus justifying the parameter selection for our core research question of regional deposition and airway structural remodeling. The CBNP volume fraction in air was less than 10%, supporting the use of a discrete phase

https://doi.org/10.1021/acs.est.5c14667
Environ. Sci. Technol. XXXX, XXX, XXX−XXX

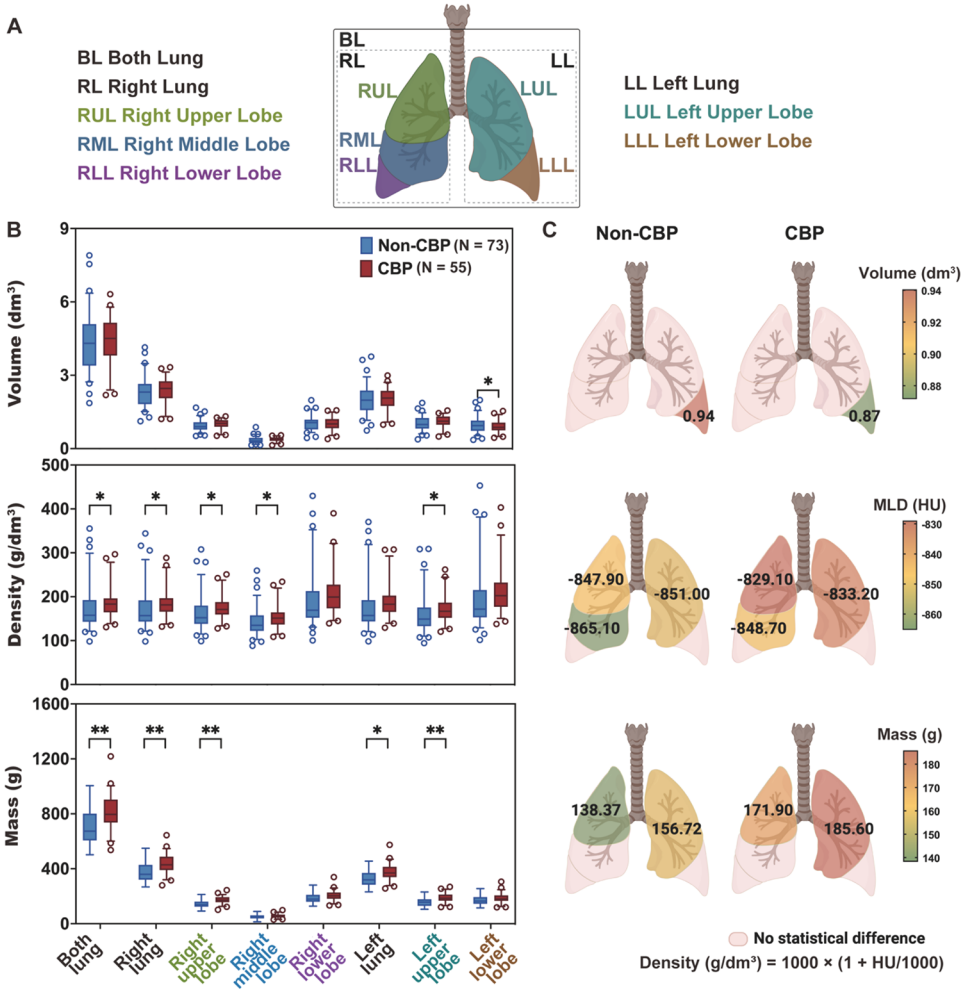

Figure 2. CBNPs increased the lung density in the upper lobes of both lungs. (A) Schematic illustration of the five lobes of the human lung. (B) Box plots of the volume, density, and mass of the whole lung and each lobe in the non-CBP and CBP groups. Density (g/dm^3) = 1000 × (1 + HU/1000) = HU + 1000. Mass is calculated as Volume × Density. HU, Hounsfield unit; Non-CBP, non carbon black packer; CBP, carbon black packer; The five horizontal lines from bottom to top represent the fifth percentile (P_5), 25th percentile (P_{25}), median, 75th percentile (P_{75}), and 95th percentile (P_{95}). Circles represent outliers. Student's *t* test (* $p < 0.05$, ** $p < 0.01$) (C) Illustration of the distributions of volume, density, and mass in the lung lobes of the non-CBP and CBP groups. MLD, mean lung density. The GLM was used to assess the associations between CBNP exposure status (categorical variable) and densitometric parameters (volume, density, and mass) with age, sex, BMI, smoking status and pack-years as covariates for adjustment.

model. The airflow velocity follows a sine curve, while anatomical parameters, including the number, length, diameter, and branch angles of the lung lobes and generations, are consistent with our previous studies[34] and are detailed in Tables S2 and S3. Considering that particles either deposit on bronchial walls or escape through inlets or outlets, the deposition fraction for each generation of the respiratory tract, $DF_{d_p,n}$, was recorded at the respiratory moment via eq 1 as follows:[36]

$$DF_{d_p,n} = \frac{DN_{d_p,n}}{TIN_{d_p}} \quad (1)$$

where d_p is the diameter of the CBNP, nm; DF_{d_p} is the deposition fraction of the CBNP of d_p, dimensionless; $DN_{d_p,n}$ is the deposited number of the CBNP of d_p in the n generation respiratory tract, dimensionless; and TIN_{d_p} is the total inhaled number of the CBNP of d_p, dimensionless. Simulations were conducted on a high-performance computing cluster (56-core Intel Xeon Gold 6330 CPU @ 2.00 GHz, 256 GB memory)[33] over approximately 14 days. Further details on the modeling procedures are provided in the Supporting Information.

2.5. Statistical Analysis

Generalized linear models (GLMs) were used to assess associations between HRCT-derived structural parameters (including densitometric parameters and airway dimension parameters) and CBNP exposure status. Age, sex, body mass index (BMI), smoking status and pack-years were selected as covariates in adjusted models. In addition, carbon content in airway macrophages (CCAM) was used as a bioeffective dosimeter for exposure to CBNP in the lungs to characterize the dose–response. GLMs were constructed to assess associations between HRCT parameters and CCAM with the same covariate adjustments. Detailed descriptions are available in the Supporting Information.

3. RESULTS AND DISCUSSION

3.1. Characterization of the Study Subjects and Exposure Assessment

Age, BMI, drinking history, and preexisting respiratory conditions were comparable between two groups. CBPs had a higher proportion of males and current smokers. The median duration of occupational exposure among CBPs was 9.5 years. Geometric mean concentrations of $PM_{2.5}$ and elemental carbon in CBNP bagging areas were significantly higher than those in

https://doi.org/10.1021/acs.est.5c14667
Environ. Sci. Technol. XXXX, XXX, XXX−XXX

Table 1. Dose−Response Relationship between the Internal Exposure to CBNPs (CCAM, Categorical) and Mean Lung Density in the Whole Lung and Each Lobe[a,b]

				all subjects (N = 82)		
MLD (HU)*	CCAM exposure group	CCAM rang (%)	interval (median (Q1, Q3))	N (CBP)	β (95% CI)	p
both lung	low CCAM	0.41−1.32	−822.50 (−836.25, −798.75)	21 (0)	REF	
	moderate CCAM	1.32−2.90	−826.30 (−839.75, −809.75)	20 (1)	−2.58 (−19.96, 14.81)	0.774
	high CCAM	2.90−9.59	−813.85 (−825.25, −800.23)	20 (11)	8.15 (−3.68, 19.98)	0.188
	very high CCAM	9.59−47.49	−800.40 (−817.20, −783.20)	21 (21)	6.34 (−1.62, 14.30)	0.128
trend					9.82 (2.77, 16.88)	**0.008**
right upper lobe	low CCAM	0.41−1.32	−850.50 (−860.10, −825.10)	21 (0)	REF	
	moderate CCAM	1.32−2.90	−852.10 (−861.88, −845.78)	20 (1)	−7.27 (−24.45, 9.92)	0.413
	high CCAM	2.90−9.59	−832.65 (−878.65, −818.85)	20 (11)	4.12 (−5.96, 14.20)	0.428
	very high CCAM	9.59−47.49	−830.50 (−839.00, −821.90)	21 (21)	3.05 (−4.49, 10.59)	0.433
trend					5.86 (−0.10, 11.82)	**0.058**
right middle lobe	low CCAM	0.41−1.32	−867.00 (−874.00, −849.60)	21 (0)	REF	
	moderate CCAM	1.32−2.90	−867.05 (−882.33, −862.90)	20 (1)	−6.54 (−20.09, 7.02)	0.351
	high CCAM	2.90−9.59	−852.35 (−863.33, −841.20)	20 (11)	7.51 (−1.90, 16.91)	0.127
	very high CCAM	9.59−47.49	−852.90 (−856.30, −837.10)	21 (21)	2.20 (−3.57, 7.97)	0.459
trend					5.77 (0.37, 11.16)	**0.039**
left upper lobe	low CCAM	0.41−1.32	−851.80 (−864.50, −831.20)	21(0)	REF	
	moderate CCAM	1.32−2.90	−855.50 (−866.70, −844.93)	20 (1)	−8.06 (−24.97, 8.86)	0.357
	high CCAM	2.90−9.59	−836.00 (−850.98, −821.35)	20 (11)	6.86 (−3.64, 17.36)	0.209
	very high CCAM	9.59−47.49	−833.20 (−848.20, −819.10)	21 (21)	3.86 (−4.18, 11.89)	0.353
trend					7.53 (1.16, 13.91)	**0.023**

[a]**Abbreviations:** CCAM = carbon content in airway macrophage; CBP = carbon black packer; Q1 = lower quartile; Q3 = upper quartile; MLD = mean lung density; HU = Hounsfield unit; 95% CI = 95% confidence interval; REF = reference. [b]GLM was used to assess the associations between internal exposure to CBNPs (CCAM, categorical) and MLD in the whole lung and each lobe with adjustments for age, sex, BMI, smoking status and pack-years. CCAM exposure groups (Low, Moderate, High, and Very high CCAM) were defined using the interquartile range (IQR) method based on the distribution of CCAM values across all study subjects (N = 82), with each group representing approximately 25% of the study population. No logarithmic transformation was conducted. MLD was selected as the outcome. The β and 95% confidence intervals (CIs) represent the differences in MLD for the Moderate, High, and Very high CCAM groups relative to the Low CCAM reference group. A trend test was performed by treating the CCAM exposure group as a continuous variable.

control areas (Table S4), and remained below recommended long-term occupational exposure limits (3.0−4.0 mg/m^3; Table S5). Previously reported measurements in this setting indicated primary particle sizes of 30−50 nm and aggregate sizes of 200−400 nm, with high specific surface area,[6] characteristics consistent with deep lung deposition.

The carbon content in airway macrophages (CCAM), a validated biomarker reflecting the internal dose of inhaled elemental carbon (EC) following chronic exposure to CBNPs and particulate matter and strongly associated with multiple adverse health outcomes.[37−40] Despite similar smoking pack-years, CCAM levels were 7.7-fold higher in CBPs than controls (Table S4), indicating that occupational CBNP exposure was the dominant contributor to pulmonary carbon burden.

3.2. Region-Specific of Increased Lung Density in CBNP-Exposed Individuals

Our previous studies revealed that CBNP inhalation alters serum biomarkers such as CC16 and surfactant protein A (SP-A), indicating lung injury in exposed workers.[7] However, these systemic biomarkers cannot location or characterize the structural changes. To address this, we applied HRCT-based lung densitometry at both whole-lung and lobar levels. Among lung density parameters, mean lung density (MLD) reflects the average density of airspaces, surrounding epithelial and extracellular matrix, and small airways, while the low attenuation areas volume percentage (LAA%) represents the proportion of lung volume with attenuation values less than −910 HU or −950 HU on end-inhalation CT scans.[41,42] These two parameters are inversely related. As shown in Figure 2, increased MLD across bilateral lungs in CBPs, with particularly pronounced effects in the upper lobes. Correspondingly, LAA% decreased in the same regions (Figure S3). Lung volume showed minimal differences between groups, whereas lung mass increased, particularly in the bilateral upper lobes (Figure 2B,C), supporting the interpretation that regional increases in lung density contributed to mass accumulation.

We further investigated the relationship between carbon content in airway macrophages (CCAM), a quantitative indicator of lung CBNP burden,[24] and lung densitometric parameters using generalized linear models in the whole lung and each lobe. Higher CCAM levels were significantly associated with increased MLD and decreased LAA% in bilateral upper lobes (Table S6). These findings indicate region-specific lung remodeling linked to internal CBNP burden.

3.3. Dose−Response Relationship Between CBNP and Lung Densitometric Parameters in the Bilateral Upper Lobes

To explore the dose−response relationship between the internal exposure dose of CBNPs and the lung density parameters, participants were stratified into four groups based on the interquartile range (IQR) of their CCAM levels. CCAM has been widely applied as a biomarker of CBNPs exposure and has been linked to respiratory and systemic health outcomes.[24,43] Generalized linear models showed monotonic increases in mean lung density (MLD) of the right middle lobe (β = 5.77 HU, $p_{\_trend}$ = 0.039), and left upper lobe (β = 7.53 HU, $p_{\_trend}$ = 0.023) with increasing CCAM, confirming a dose−response relationship between CCAM and MLD in the bilateral upper lobes (Table 1). In contrast, low attenuation areas volume

https://doi.org/10.1021/acs.est.5c14667
Environ. Sci. Technol. XXXX, XXX, XXX−XXX

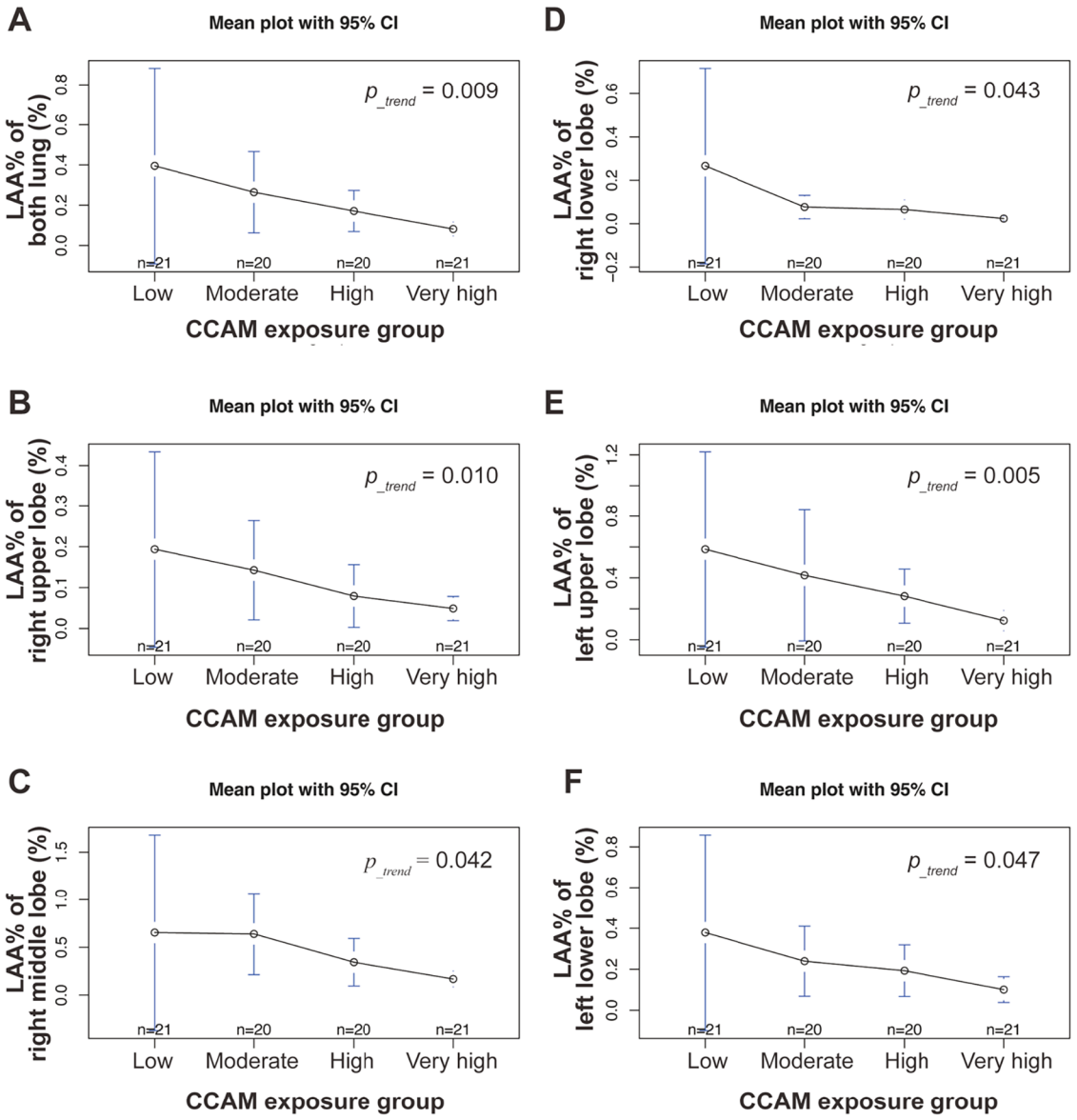

Figure 3. Dose−response relationship between internal exposure to CBNPs (CCAM, categorical) and LAA% in the whole lung and each lobe. GLM assessed the associations between internal exposure to CBNPs (CCAM, categorical) and LAA% in the whole lung and each lobe with adjustment of age, sex, BMI, smoking status and packyears. No logarithmic transformation was conducted. LAA% was selected as the outcome. CCAM exposure groups were defined by the interquartile range (IQR) of CCAM levels across all study subjects (N = 82), with exact ranges: Low (0.41−1.32%, reference group), Moderate (1.32−2.90%), High (2.90−9.59%), and Very high CCAM (9.59−47.49%). The β and 95% confidence intervals (CIs) represent the differences in LAA% for the Moderate, High, and Very high CCAM groups relative to the Low CCAM reference group. Trend test was performed by treating the CCAM exposure group as a continuous variable.

percentage (LAA%) across the bilateral lungs showed monotonic decreases with increasing CCAM (all $p_{\_trend}$ values $\leq$ 0.047, Figure 3). These results demonstrate a dose−response relationship between pulmonary deposition of CBNP and increased lung density in the bilateral upper lobes, supporting a cumulative structural impact of long-term exposure.

3.4. Generation- and Region-Specific of Airway Wall Thickening in CBNP-Exposed Individuals

Early increases in lung density may reflect lung injury or inflammatory processes and are often accompanied by structural changes in the small airways, including airway wall thickening.[44] Because small airways are typically the first anatomical sites impacted by inhaled environmental pollutants, they represent a critical target for investigating early lung injury.[45] Compared with controls, the airway wall area percentage (WA%) in sixth generation bronchi was significantly greater in the right B1, right B9, left B1 + 2, and left B9 to carina among CBPs. In contrast, changes in ninth generation bronchi were weaker and limited to left B1 + 2 to carina, with other segments showed nonsignificant upward trends (Figure 4). The most pronounced thickening in both generations was occurred in the left upper lobe, consistent with the regional pattern of increased lung density.

Generalized linear model (GLM) analysis revealed significant associations between internal CBNPs burden (CCAM) and WA % in the sixth generation bronchi of right B1, left B1 + 2, and left B9 to carina (Table S7). The greatest airway wall thickening occurred in the left lower lobe, followed by the bilateral upper lobes. Associations in the ninth generation bronchi were limited to the left B1 + 2 to carina (Table S7) and were weaker.

https://doi.org/10.1021/acs.est.5c14667
Environ. Sci. Technol. XXXX, XXX, XXX−XXX

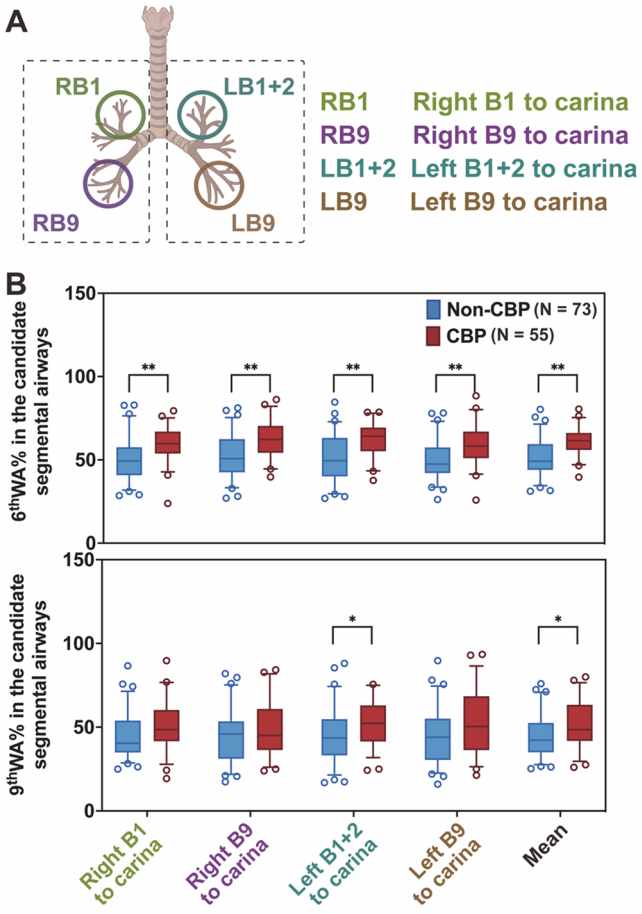

Figure 4. Susceptible regions of small airway wall thickening in the 6th- and 9th-generation bronchi due to CBNP exposure. (A) Schematic representation of the four candidate lung segments in separate lobes bilaterally that run orthogonal to the axial plane were selected, including RB1, RB9, LB1 + 2, and LB9. (B) Box plots of WA% in the 6th- and 9th-generation bronchi for the four candidate lung segments in the Non-CBP and CBP groups. The horizontal lines from bottom to top represent the fifth percentile (P_5), 25th percentile (P_{25}), median, 75th percentile (P_{75}), and 95th percentile (P_{95}). The circles indicate outliers. Non-CBP, non carbon black packer; CBP, carbon black packer; WA%, airway wall area percentage; Q1, lower quartile; Q3, upper quartile; Mean, the average WA% for the same bronchial generation across the four selected lung segments; 95% CI, 95% confidence interval. The means indicate the average WA% for the same bronchial generation across the four selected lung segments. GLM was used to assess the associations between CBNP exposure status (categorical variable) and WA% in the 6th- and 9th-generation bronchi with age, sex, BMI, smoking status and pack-years as covariates for adjustment (* $p < 0.05$, ** $p < 0.01$).

Together, these findings indicate that CBNP exposure preferentially induces airway wall thickening in proximal small airways, particularly in the bilateral upper lobes, consistent with the observed region-specific increases in lung density.

3.5. Dose−Response Relationship Between CBNP and WA% in Proximal Small Airways of Upper Lobe

Generalized linear model (GLM) analysis using CCAM quartiles further demonstrated a clear dose−response relationship between internal CBNP burden and airway wall area percentage (WA%) in sixth generation bronchi of the right B1, left B1 + 2, and left B9 to carina, as well as in the average WA% across these four segments. No significant dose−response relationship was detected in the ninth generation bronchi (Table 2). These results indicate that CBNP exposure preferentially induces dose−dependent airway wall thickening in proximal small airways of the bilateral upper lobes. Similar region-specific susceptibility to airway wall thickening in the right upper lobe has been reported among particulate matter-exposed tollbooth workers.[46] We additionally examined the association between the duration of occupational CBNP exposure and HRCT-derived parameters. Longer occupational exposure duration was associated with increased lung density (higher mean lung density and lower LAA%) in the bilateral upper lobes and with elevated WA% mainly in sixth generation bronchi, whereas associations in ninth generation bronchi were limited (Table S8). Compared with exposure duration, CCAM showed stronger and more consistent relationships with both lung densitometric and airway structural parameters, underscoring the value of macrophage-based internal dose metrics (CCAM) in capturing cumulative biologically effective exposure.

Smoking-stratified analysis suggested that smoking may influence CBNP-induced pulmonary injury, blunting CBNP-associated lung density elevation and ninth generation airway wall thickening in current smokers. Notably, CBNP-induced sixth generation proximal small airway thickening was smoking-independent, with the bilateral upper lobe vulnerability pattern preserved in never smokers (Table S9). These findings support the proximal small airway as a key vulnerable site for CBNP exposure independent of smoking, help rule out smoking as a major confounding variable for our results, and indicate that never smokers may represent a susceptible population in whom CBNP-induced subclinical lung remodeling can be more readily detected.

3.6. Computational Modeling Reveals CBNP Deposition-Driven Vulnerability in Lung Lobes

Building on prior evidence that similar sized nanoparticles tend to concentrate in proximal airways,[47] we hypothesized predominant CBNP deposition in proximal (6th generation) small airways. A laminar flow-based model was applied to simulate CBNP transport and deposition across ten airway generations (from the first to the 10th generation) and five lung lobes (Figure S2), with lobe-volume normalization. Computational simulations indicated predominant CBNP deposition in the right upper lobe (206.57 m^{-3}), left upper lobe (170.22 m^{-3}) and left lower lobe (218.71 m^{-3}), whereas deposition was lowest in the right middle lobe (Figure 5A). Notably, the bilateral upper lobes the highest deposition rates, closely mirroring HRCT-detected increases in lung density and airway wall thickening in CBNP-exposed workers. The relatively elevated deposition predicted in the left lower lobe may reflect geometric simplifications in the model, which could underestimate dispersion in this region. Generation-specific analyses showed greater deposition in proximal than distal small airways across lobes (Figure 5B−G). This pattern is consistent with particle transport dominated by inertial impaction and Brownian motion in larger proximal airways, whereas Brownian motion becomes the primary mechanism in smaller distal bronchi. Preferential deposition in the bilateral upper lobes can be explained by higher airflow velocity and branching geometry that enhance inertial impaction in upper-lobe proximal airways. Consistent with our prior vortex-ring simulations in acinar regions,[47] deposition scores were higher in the bilateral upper lobes (16.7%) than in the lower lobes (11.5%, Figure 5H), reinforcing their role as regional vulnerability hotspots. Importantly, the region- and

https://doi.org/10.1021/acs.est.5c14667
Environ. Sci. Technol. XXXX, XXX, XXX−XXX

Table 2. Dose−Response Relationship between Internal Exposure to CBNPs (CCAM, categorical) and WA% in the 6th- and 9th-Generation Bronchi[a,b]

					all subjects (N = 82)	
variable	CCAM exposure group	CCAM rang (%)	interval (median (Q1, Q3))	N (CBP)	β (95% CI)	p
6th WA%						
right B1 to carina	low CCAM	0.41−1.32	45.57 (39.07, 51.41)	21 (0)	REF	
	moderate CCAM	1.32−2.90	52.63 (44.80, 60.74)	20 (1)	7.86 (1.04, 14.68)	0.031
	high CCAM	2.90−9.59	51.82 (46.62, 55.36)	20 (11)	3.27 (−0.45, 6.99)	0.096
	very high CCAM	9.59−47.49	59.38 (53.85, 66.16)	21 (21)	4.77 (2.34, 7.19)	0.001
trend					4.25 (1.82, 6.67)	**0.001**
left B1 + 2 to carina	low CCAM	0.41−1.32	46.97 (41.04, 58.98)	21 (0)	REF	
	moderate CCAM	1.32−2.90	50.25 (42.32, 62.19)	20 (1)	3.06 (−4.89, 11.02)	0.456
	high CCAM	2.90−9.59	55.44 (48.68, 63.16)	20 (11)	3.05 (−1.27, 7.38)	0.177
	very high CCAM	9.59−47.49	64.22 (52.20, 69.48)	21 (21)	3.49 (0.37, 6.60)	0.035
trend					3.61 (1.02, 6.19)	**0.008**
left B9 to carina	low CCAM	0.41−1.32	44.17 (39.65, 52.31)	21 (0)	REF	
	moderate CCAM	1.32−2.90	46.13 (41.91, 58.27)	20 (1)	3.53 (−2.48, 9.54)	0.259
	high CCAM	2.90−9.59	55.80 (48.54, 57.02)	20 (11)	4.24 (1.58, 6.89)	0.004
	very high CCAM	9.59−47.49	58.93 (50.96, 66.27)	21 (21)	3.85 (0.88, 6.82)	0.016
trend					3.98 (1.60, 6.37)	**0.002**
mean	low CCAM	0.41−1.32	49.17 (44.33, 52.41)	21 (0)	REF	
	moderate CCAM	1.32−2.90	49.96 (43.57, 58.12)	20 (1)	3.11 (−1.91, 8.14)	0.234
	high CCAM	2.90−9.59	55.51 (47.13, 59.14)	20 (11)	3.01 (0.03, 5.99)	0.057
	very high CCAM	9.59−47.49	57.94 (55.37, 66.18)	21 (21)	3.65 (1.38, 5.93)	0.004
trend					3.64 (1.71, 5.57)	**<0.001**
9th WA%						
left B1 + 2 to carina	low CCAM	0.41−1.32	35.85 (31.41, 52.50)	21 (0)	REF	
	moderate CCAM	1.32−2.90	42.86 (35.80, 52.17)	20 (1)	1.39 (−8.29, 11.08)	0.780
	high CCAM	2.90−9.59	40.61 (35.52, 44.83)	20 (11)	−0.04 (−5.30, 5.22)	0.988
	very high CCAM	9.59−47.49	46.27 (44.00, 60.00)	21 (21)	3.05 (−0.83, 6.93)	0.132
trend					2.85 (−0.15, 5.86)	**0.067**

[a]**Abbreviations:** CCAM = carbon content in airway macrophage; CBP = carbon black packer; WA% = airway wall area percentage; Q1 = lower quartile; Q3 = upper quartile; mean = the average WA% for the same bronchial generation across the four selected lung segments; 95% CI = 95% confidence interval; REF = reference.. [b]GLM was used to assess the associations between internal exposure to CBNPs (CCAM, categorical) and WA% in the 6th- and 9th-generation bronchi of the candidate segmental airways with adjustments for age, sex, BMI, smoking status and pack-years. CCAM exposure groups (Low, Moderate, High, and Very high CCAM) were defined using the interquartile range (IQR) method based on the distribution of CCAM values across all study subjects (N = 82), with each group representing approximately 25% of the study population. No logarithmic transformation was conducted. The WA% of the 6th and 9th generation bronchi in the four candidate lung segments, RB1, RB9, LB1 + 2, and LB9, was used as the outcome. The β and 95% confidence intervals (CIs) represent the differences in WA% for the Moderate, High, and Very high CCAM groups relative to the Low CCAM reference group. A trend test was performed by treating the CCAM exposure group as a continuous variable.

generation-specific deposition patterns predicted by the model closely mirrored HRCT-derived increases in lung density and airway wall thickening in CBNP-exposed workers. These concordant findings support a deposition-driven mechanism in which preferential CBNP accumulation in proximal small airways and bilateral upper lobes promotes localized remodeling.

3.7. Environmental Implications and Study Limitations

CT-detected increases in lung density and airway wall thickening are widely regarded as a structural biomarker of lung remodeling, reflecting epithelial injury, inflammatory cell infiltration, and extracellular matrix deposition.[48−50] Preferential CBNP deposition in proximal small airways may impair clearance, enhance macrophage-mediated inflammation responses, thereby promoting localized airway remodeling. In the present study, preferential CBNP deposition in proximal small airways and upper lung regions was accompanied by spatially localized structural alterations, suggesting that particle deposition patterns may define anatomically susceptible sites of early remodeling. Unlike previous human studies of particulate exposure that predominantly relied on pulmonary function testing, our analysis provides *in vivo*, region-resolved evidence linking internal CBNP exposure metrics (CCAM) and computational deposition modeling with quantitative structural imaging changes. These findings support a deposition-driven pathogenic pathway that may contribute to the early development of small-airway disease and chronic obstructive pulmonary disease, and highlight the importance of incorporating spatial deposition characteristics and imaging-based biomarkers into nanotoxicology and environmental health risk assessment frameworks. Notably, significant early structural lung alterations were detected in carbon black packers at CBNP exposure levels well below the established 8-h time-weighted average (TWA) occupational exposure limits (OELs, 3.0−4.0 mg/m^3). These OELs are primarily established based on acute toxicity outcomes and pulmonary function indices (e.g., FEV1) from long-term occupational exposure studies, with no consideration for the chronic, low-dose subclinical structural remodeling induced by CBNPs. Our findings thus highlight the urgent need to re-evaluate and refine existing CBNP OELs, incorporating imaging-based biomarkers of early lung structural injury to

https://doi.org/10.1021/acs.est.5c14667
Environ. Sci. Technol. XXXX, XXX, XXX−XXX

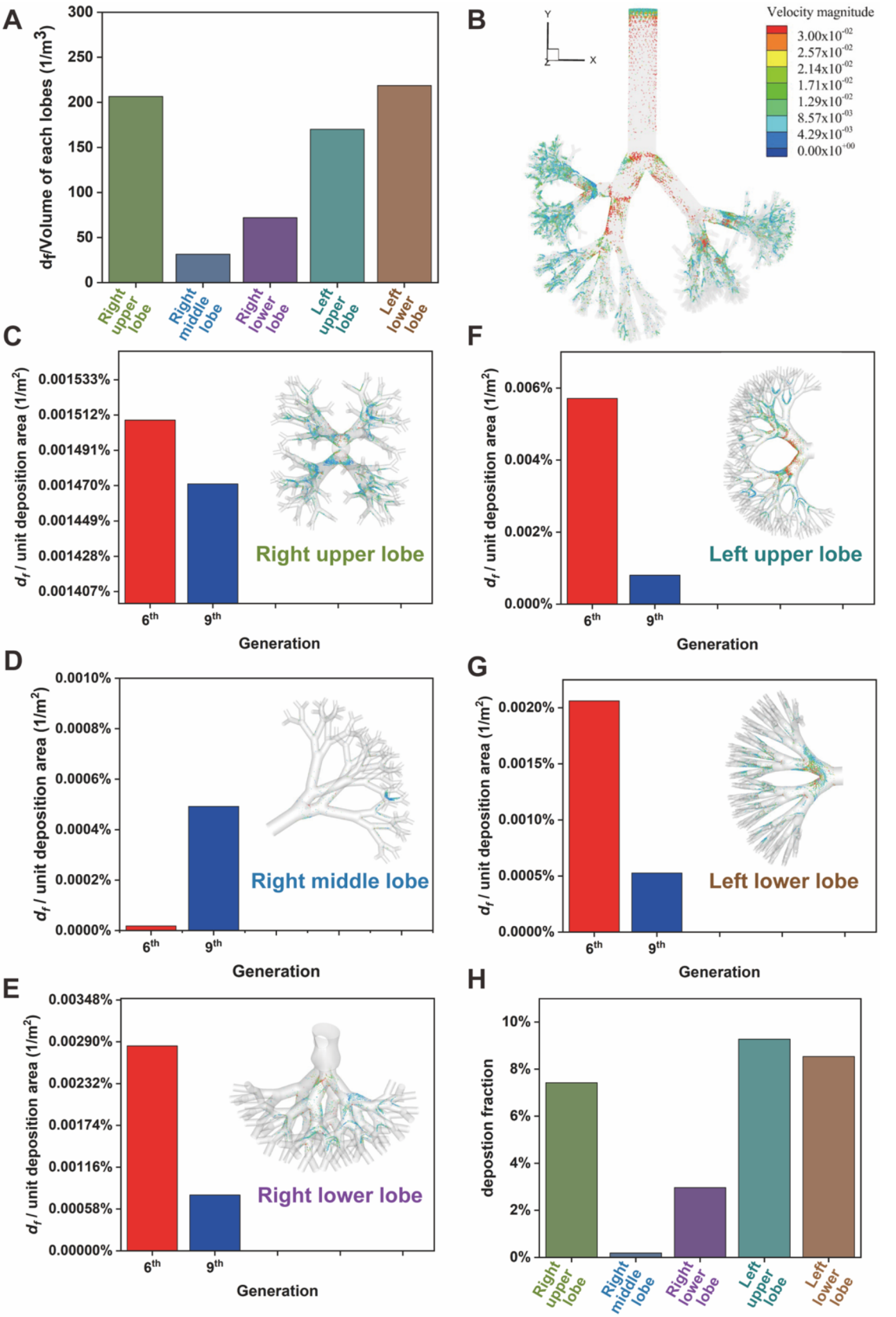

Figure 5. CBNP deposition characteristics in each lobe. (A) Histogram of the deposition fraction per unit volume of each lobe. (B) Deposition positions of CBNPs. (C-G) Histogram of the deposition fraction per deposition area and particle deposition distribution in the 6th- and 9th-generation bronchi. (H) Histogram of the deposition fraction of pulmonary acini in each lobe.

https://doi.org/10.1021/acs.est.5c14667
Environ. Sci. Technol. XXXX, XXX, XXX−XXX

better protect occupational populations from subclinical small airway damage.

Despite these important insights, several limitations of our study warrant acknowledgment. Given its cross-sectional design, definitive causal inference cannot be established. Nevertheless, the consistent dose−response relationships observed across CBNP internal exposure metrics, quantitative imaging biomarkers, and regional deposition modeling provide supportive evidence for a biologically plausible association, thereby partially strengthening the inferential robustness of the findings. In addition, our computational fluid dynamic (CFD)-based CBNP deposition model has inherent simplifications: we used a representative uniform respirable particle size from workplace characterization rather than a polydisperse distribution, and did not incorporate pretracheal turbulent flow or respiratory tract clearance mechanisms (e.g., mucociliary transport). Future studies could refine predictions by integrating these more realistic particle distribution and physiological factors. Furthermore, minor variability in quantitative HRCT measurements may exist due to individual tracheobronchial anatomical differences, consistent with current literature and without impacting our core findings.

In summary, long-term CBNP inhalation induces region- and generation-specific lung remodeling, with preferential deposition and structural alterations in the bilateral upper lobes and proximal small airways. This deposition-driven vulnerability underscores the utility of imaging-based biomarkers for early detection and provides mechanistic insights to inform risk assessment and preventive strategies for nanomaterial-related lung injury in occupational and environmental settings.

■ ASSOCIATED CONTENT

Supporting Information

The Supporting Information is available free of charge at https://pubs.acs.org/doi/10.1021/acs.est.5c14667.

These detailed methods (CCAM assay, quantitative HRCT assessment of lung density and airway dimension parameters, and mathematical model and methodology) (PDF)

■ AUTHOR INFORMATION

Corresponding Authors

Wei Han − *Department of Occupational and Environmental Health, School of Public Health, Qingdao University, Qingdao 266071 Shandong, China; Department of Respiratory and Critical Care Medicine, Qingdao Municipal Hospital, School of Medicine, Qingdao University, Qingdao 266071 Shandong, China*; Email: hanw@qdu.edu.cn

Yingxin Yu − *Guangdong Key Laboratory of Environmental Catalysis and Health Risk Control, Guangdong- Hong Kong-Macao Joint Laboratory for Contaminants Exposure and Health, Institute of Environmental Health and Pollution Control, School of Environmental Science and Engineering, Guangdong University of Technology, Guangzhou 510006 Guangdong,, China*; orcid.org/0000-0001-8736-3821; Email: yuyingxin@gdut.edu.cn

Jinglong Tang − *Department of Occupational and Environmental Health, School of Public Health, Qingdao University, Qingdao 266071 Shandong, China*; orcid.org/0000-0001-9981-7966; Email: tangjinglong@qdu.edu.cn

Authors

Wenting Cheng − *Department of Biotherapy, Oxidative Stress Research Center, Cancer Center and State Key Laboratory of Biotherapy, West China Hospital, Sichuan University, Chengdu 610041 Sichuan, China; Department of Occupational and Environmental Health, School of Public Health, Qingdao University, Qingdao 266071 Shandong, China*

Zijian Ma − *Guangdong Key Laboratory of Environmental Catalysis and Health Risk Control, Guangdong- Hong Kong-Macao Joint Laboratory for Contaminants Exposure and Health, Institute of Environmental Health and Pollution Control, School of Environmental Science and Engineering, Guangdong University of Technology, Guangzhou 510006 Guangdong,, China*

Xinyi Zhang − *Department of Occupational and Environmental Health, School of Public Health, Qingdao University, Qingdao 266071 Shandong, China*

Yuxin Zheng − *Department of Occupational and Environmental Health, School of Public Health, Qingdao University, Qingdao 266071 Shandong, China*

Complete contact information is available at: https://pubs.acs.org/10.1021/acs.est.5c14667

Author Contributions

⊥W.C. and Z.M. contributed equally to this work.

Funding

This work was supported by the National Natural Science Foundation of China (82241086, 82273669, and 82574147) and the Postdoctoral Research Project, West China Hospital, Sichuan University (2025HXBH072).

Notes

The authors declare no competing financial interest.

■ ACKNOWLEDGMENTS

The authors would like to thank Dr. Yufei Dai and Dr. Huawei Duan from the Chinese Centers for Disease Control and Prevention for their assistance in cohort maintenance and Xiaofa Yang and Haisheng Wang from the Luoyang and Jiaozuo Centers for Disease Control and Prevention for their assistance in the field study. We also thank Dr. Shuguang Leng of New Mexico University for assisting with the data analysis.

■ REFERENCES

(1) World Health Organization*WHO Guidelines on Protecting Workers from Potential Risks of Manufactured Nanomaterials.*; World Health Organization: Geneva, Switzerland, 2017; p 29.

(2) International Carbon Black Association. *Carbon black user's guide*, 2024 https://www.carbon-black.org/resources-from-icba (accessed April 2, 2026), pp. 1−35.

(3) McCunney, R. J.; Levy, L.; Chaudhuri, I.; Ngiewih, Y.; Yong, M.; Wampler, W.Carbon Black. In *Patty's Toxicology* 2003; pp 1−25.

(4) Zhang, X. L.; Li, S.; Wang, S. H.; Wang, Z. X.; Wen, Z. S.; Ji, S. J.; Sun, J. C. An amorphous hierarchical MnO(2)/acetylene black composite with boosted rate performance as an anode for lithium-ion batteries. *Dalton Trans.* **2021**, *50* (31), 10749−10757.

(5) Liu, Y. T.; Zhang, R. H.; Wang, J.; Wang, Y. Current and future lithium-ion battery manufacturing. *iScience* **2021**, *24* (4), No. 102332.

(6) Zhang, R.; Dai, Y.; Zhang, X.; Niu, Y.; Meng, T.; Li, Y.; Duan, H.; Bin, P.; Ye, M.; Jia, X.; et al. Reduced pulmonary function and increased pro-inflammatory cytokines in nanoscale carbon black-exposed workers. *Part. Fibre Toxicol.* **2014**, *11*, No. 73.

(7) Yang, M.; Li, Y.; Meng, T.; Zhang, L.; Niu, Y.; Dai, Y.; Gao, W.; Bloom, M. S.; Dong, G.; Zheng, Y. Ultrafine CB-induced small airway obstruction in CB-exposed workers and mice. *Sci. Total Environ.* **2019**, *671*, 866−873.
(8) Cao, X.; Lin, L.; Sood, A.; Ma, Q.; Zhang, X.; Liu, Y.; Liu, H.; Li, Y.; Wang, T.; Tang, J.; et al. Small Airway Wall Thickening Assessed by Computerized Tomography Is Associated With Low Lung Function in Chinese Carbon Black Packers. *Toxicol. Sci.* **2020**, *178* (1), 26−35.
(9) Schaffenrath, J.; Wyss, T.; He, L.; Rushing, E.; Delorenzi, M.; Vasella, F.; Regli, L.; Neidert, M.; Keller, A. Blood-brain barrier alterations in human brain tumors revealed by genome-wide transcriptomic profiling. *Neuro-Oncol.* **2021**, *23* (12), 2095−2106, DOI: 10.1093/neuonc/noab022.
(10) Chang, C. Y.; You, R.; Armstrong, D.; Bandi, A.; Cheng, Y. T.; Burkhardt, P. M.; Becerra-Dominguez, L.; Madison, M. C.; Tung, H. Y.; Zeng, Z.; et al. Chronic exposure to carbon black ultrafine particles reprograms macrophage metabolism and accelerates lung cancer. *Sci. Adv.* **2022**, *8* (46), No. eabq0615.
(11) Galbán, C. J.; Han, M. K.; Boes, J. L.; Chughtai, K. A.; Meyer, C. R.; Johnson, T. D.; Galbán, S.; Rehemtulla, A.; Kazerooni, E. A.; Martinez, F. J.; Ross, B. D. Computed tomography-based biomarker provides unique signature for diagnosis of COPD phenotypes and disease progression. *Nat. Med.* **2012**, *18* (11), 1711−1715.
(12) Boudewijn, I. M.; Postma, D. S.; Telenga, E. D.; Ten Hacken, N. H.; Timens, W.; Oudkerk, M.; Ross, B. D.; Galbán, C. J.; van den Berge, M. Effects of ageing and smoking on pulmonary computed tomography scans using parametric response mapping. *Eur. Respir. J.* **2015**, *46* (4), 1193−1196.
(13) Kirby, M.; Tanabe, N.; Tan, W. C.; Zhou, G.; Obeidat, M.; Hague, C. J.; Leipsic, J.; Bourbeau, J.; Sin, D. D.; Hogg, J. C.; Coxson, H. O. Total Airway Count on Computed Tomography and the Risk of Chronic Obstructive Pulmonary Disease Progression. Findings from a Population-based Study. *Am. J. Respir. Crit. Care Med.* **2018**, *197* (1), 56−65.
(14) Verleden, S. E.; Hendriks, J. M. H.; Snoeckx, A.; Mai, C.; Mentens, Y.; Callebaut, W.; De Belie, B.; Van Schil, P. E.; Verplancke, V.; Janssens, A.; et al. Small Airway Disease in Pre-Chronic Obstructive Pulmonary Disease with Emphysema: A Cross-Sectional Study. *Am. J. Respir. Crit. Care Med.* **2024**, *209* (6), 683−692.
(15) Tanabe, N.; Vasilescu, D. M.; Kirby, M.; Coxson, H. O.; Verleden, S. E.; Vanaudenaerde, B. M.; Kinose, D.; Nakano, Y.; Paré, P. D.; Hogg, J. C. Analysis of airway pathology in COPD using a combination of computed tomography, micro-computed tomography and histology. *Eur. Respir. J.* **2018**, *51* (2), No. 1701245, DOI: 10.1183/13993003.01245-2017.
(16) Mascalchi, M.; Camiciottoli, G.; Diciotti, S. Lung densitometry: why, how and when. *J. Thorac. Dis.* **2017**, *9* (9), 3319−3345.
(17) Lu, J.; Ge, H.; Qi, L.; Zhang, S.; Yang, Y.; Huang, X.; Li, M. Subtyping preserved ratio impaired spirometry (PRISm) by using quantitative HRCT imaging characteristics. *Respir. Res.* **2022**, *23* (1), No. 309.
(18) Ashraf, H.; Lo, P.; Shaker, S. B.; de Bruijne, M.; Dirksen, A.; Tønnesen, P.; Dahlbäck, M.; Pedersen, J. H. Short-term effect of changes in smoking behaviour on emphysema quantification by CT. *Thorax* **2011**, *66* (1), 55−60.
(19) Shaker, S. B.; Dirksen, A.; Lo, P.; Skovgaard, L. T.; de Bruijne, M.; Pedersen, J. H. Factors influencing the decline in lung density in a Danish lung cancer screening cohort. *Eur. Respir. J.* **2012**, *40* (5), 1142−1148.
(20) Liu, H.; Li, J.; Ma, Q.; Tang, J.; Jiang, M.; Cao, X.; Lin, L.; Kong, N.; Yu, S.; Sood, A.; et al. Chronic exposure to diesel exhaust may cause small airway wall thickening without lumen narrowing: a quantitative computerized tomography study in Chinese diesel engine testers. *Part. Fibre Toxicol.* **2021**, *18* (1), 14.
(21) McDonough, J. E.; Yuan, R.; Suzuki, M.; Seyednejad, N.; Elliott, W. M.; Sanchez, P. G.; Wright, A. C.; Gefter, W. B.; Litzky, L.; Coxson, H. O.; et al. Small-airway obstruction and emphysema in chronic obstructive pulmonary disease. *N. Engl. J. Med.* **2011**, *365* (17), 1567−1575.
(22) Tanabe, N. Increase Attention to Computed Tomography Findings of Emphysema without Airflow Limitation: Small Airway Disease Is Already There. *Am. J. Respir. Crit. Care Med.* **2024**, *209* (6), 619−621.
(23) Yang, M.; Li, Y.; Meng, T.; Zhang, L.; Niu, Y.; Dai, Y.; Gao, W.; Bloom, M.; Dong, G.; Zheng, Y. Ultrafine CB-induced small airway obstruction in CB-exposed workers and mice. *Sci. Total Environ.* **2019**, *671*, 866−873.
(24) Cheng, W.; Liu, Y.; Tang, J.; Duan, H.; Wei, X.; Zhang, X.; Yu, S.; Campen, M.; Han, W.; Rothman, N.; et al. Carbon content in airway macrophages and genomic instability in Chinese carbon black packers. *Arch. Toxicol.* **2020**, *94* (3), 761−771.
(25) Dai, Y.; Niu, Y.; Duan, H.; Bassig, B. A.; Ye, M.; Zhang, X.; Meng, T.; Bin, P.; Jia, X.; Shen, M.; et al. Effects of occupational exposure to carbon black on peripheral white blood cell counts and lymphocyte subsets. *Environ. Mol. Mutagen.* **2016**, *57* (8), 615−622.
(26) Sun, H.; Cheng, W. T.; Zhang, X. Y.; Sun, Z. L.; Sun, H. W.; Tian, S. H.; Tang, J. L. Measuring Carbon Content in Airway Macrophages Exposed to Carbon-Containing Particulate Matters. *J. Vis. Exp.* **2024**, *209*, No. e66781, DOI: 10.3791/66781.
(27) Lutey, B. A.; Conradi, S. H.; Atkinson, J. J.; Zheng, J.; Schechtman, K. B.; Senior, R. M.; Gierada, D. S. Accurate measurement of small airways on low-dose thoracic CT scans in smokers. *Chest* **2013**, *143* (5), 1321−1329.
(28) Karimi, R.; Tornling, G.; Forsslund, H.; Mikko, M.; Wheelock, Å.; Nyrén, M.; Sköld, C. M. C. M. Differences in regional air trapping in current smokers with normal spirometry. *Eur. Respir. J.* **2017**, *49* (1), No. 1600345, DOI: 10.1183/13993003.00345-2016.
(29) Atzeni, C.; Lesma, G.; Dubini, G.; Masi, M.; Rossi, F.; Bianchi, E. Computational fluid dynamic models as tools to predict aerosol distribution in tracheobronchial airways. *Sci. Rep.* **2021**, *11* (1), No. 1109.
(30) Islam, M. S.; Larpruenrudee, P.; Paul, A. R.; Paul, G.; Gemci, T.; Gu, Y.; Saha, S. C. SARS CoV-2 aerosol: How far it can travel to the lower airways? *Phys. Fluids* **2021**, *33* (6), No. 061903.
(31) Islam, M. S.; Larpruenrudee, P.; Saha, S. C.; Pourmehran, O.; Paul, A. R.; Gemci, T.; Collins, R.; Paul, G.; Gu, Y. How severe acute respiratory syndrome coronavirus-2 aerosol propagates through the age-specific upper airways. *Phys. Fluids* **2021**, *33* (8), No. 081911.
(32) Ciloglu, D. Numerical simulation of the unsteady flow field in the human pulmonary acinus. *Sādhanā* **2021**, *46* (4), No. 186, DOI: 10.1007/s12046-021-01704-2.
(33) Ansys, I. *ANSYS Fluent Theory Guide* 2020.
(34) Zhuang, Y. J.; Ma, Z. J.; Long, X. A.; Yang, Y.; Yu, Y. X. Numerical simulation on deposition effects of ultrafine particles in the asymmetrical lower respiratory tract. *Chin. Sci. Bull.* **2021**, *66* (31), 4054−4064.
(35) Chen, C.; Zhao, B. A modified Brownian force for ultrafine particle penetration through building crack modeling. *Atmos. Environ.* **2017**, *170*, 143−148.
(36) Zhang, Z.; Kleinstreuer, C.; Kim, C. S. Comparison of analytical and CFD models with regard to micron particle deposition in a human 16-generation tracheobronchial airway model. *J. Aerosol. Sci.* **2009**, *40* (1), 16−28.
(37) Bai, Y.; Casas, L.; Scheers, H.; Janssen, B. G.; Nemery, B.; Nawrot, T. S. Mitochondrial DNA content in blood and carbon load in airway macrophages. A panel study in elderly subjects. *Environ. Int.* **2018**, *119*, 47−53.
(38) Jacobs, L.; Emmerechts, J.; Mathieu, C.; Hoylaerts, M. F.; Fierens, F.; Hoet, P. H.; Nemery, B.; Nawrot, T. S. Air pollution related prothrombotic changes in persons with diabetes. *Environ. Health Perspect.* **2010**, *118* (2), 191−196.
(39) Bai, Y.; Bove, H.; Nawrot, T. S.; Nemery, B. Carbon load in airway macrophages as a biomarker of exposure to particulate air pollution; a longitudinal study of an international Panel. *Part. Fibre Toxicol.* **2018**, *15* (1), No. 14.
(40) Tang, J.; Cheng, W.; Gao, J.; Li, Y.; Yao, R.; Rothman, N.; Lan, Q.; Campen, M.; Zheng, Y.; Leng, S. Occupational exposure to carbon black nanoparticles increases inflammatory vascular disease risk: an

implication of an ex vivo biosensor assay. *Part. Fibre Toxicol.* **2020**, *17* (1), No. 47.
(41) Tran, H. M.; Chen, T. T.; Lu, Y. H.; Tsai, F. J.; Chen, K. Y.; Ho, S. C.; Wu, C. D.; Wu, S. M.; Lee, Y. L.; Chung, K. F.; et al. Climate-mediated air pollution associated with COPD severity. *Sci. Total Environ.* **2022**, *843*, No. 156969.
(42) Abadi, E.; Jadick, G.; Lynch, D. A.; Segars, W. P.; Samei, E. Emphysema Quantifications With CT Scan: Assessing the Effects of Acquisition Protocols and Imaging Parameters Using Virtual Imaging Trials. *Chest* **2023**, *163* (5), 1084−1100.
(43) Kulkarni, N.; Pierse, N.; Rushton, L.; Grigg, J. Carbon in airway macrophages and lung function in children. *N. Engl. J. Med.* **2006**, *355* (1), 21−30.
(44) Pompe, E.; Strand, M.; van Rikxoort, E. M.; Hoffman, E. A.; Barr, R. G.; Charbonnier, J. P.; Humphries, S.; Han, M. K.; Hokanson, J. E.; Make, B. J.; et al. Five-year Progression of Emphysema and Air Trapping at CT in Smokers with and Those without Chronic Obstructive Pulmonary Disease: Results from the COPDGene Study. *Radiology* **2020**, *295* (1), 218−226.
(45) Hogg, J. C.; Timens, W. The pathology of chronic obstructive pulmonary disease. *Annu. Rev. Pathol.* **2009**, *4*, 435−459.
(46) Safak, A. A.; Arbak, P.; Yazici, B.; Bilgin, C.; Erdogmus, B.; Annakkaya, A. N.; Ozsahin, S. L. Bronchial wall thickness in toll collectors. *Ind. Health* **2010**, *48* (3), 317−323.
(47) Yang, Y.; Ma, Z.; Zhuang, Y.; Long, X.; Yu, Y. Development of multi-generation lower respiratory tract model and insights into the transport and deposition characteristics of inhalable particles. *Sci. Total Environ.* **2023**, *904*, No. 166725.
(48) Hogg, J. C. Pathophysiology of airflow limitation in chronic obstructive pulmonary disease. *Lancet* **2004**, *364* (9435), 709−721.
(49) Sermet-Gaudelus, I.; Letierce, A.; Berteloot, L.; Bonnel, A.-S.; Chen, Y.; Makani, P.; Kelly-Aubert, M.; Kanoun, F.; Penalva, L.; Bouleghem, N.; et al. Effect of elexacaftor-tezacaftor-ivacaftor on bronchial dilatations in adolescents with cystic fibrosis: a multicentre prospective observati onal study. *Lancet Respir. Med.* **2026**, *14* (1), 38−48.
(50) Guo, X.; Chen, J.; Zhao, Q.; Liu, Y.; Wang, X. ^{18}F-FAPI versus ^{18}F-FDG PET/CT in the Diagnosis of Relapsing Polychondritis. *Clin. Case Rep.* **2024**, *12* (12), No. e9690.

https://doi.org/10.1021/acs.est.5c14667
Environ. Sci. Technol. XXXX, XXX, XXX−XXX